Journal of Inorganic Biochemistry 249 (2023) 112386

Contents lists available at ScienceDirect

Journal of Inorganic Biochemistry

journal homepage: www.elsevier.com/locate/jinorgbio

Iron(II)-cyclopentadienyl compounds are cytotoxic against colon adenocarcinoma cell lines: Ethylenebis(diphenylphosphane) vs. triphenylphosphane

Adhan Pilon [a], Fernando Avecilla [b], Bálint Rácz [c], Gerda T. Gátszegi [c,d], Gabriella Spengler [c], M. Paula Robalo [e,f], Éva A. Enyedy [d], M. Helena Garcia [a,*], Andreia Valente [a,*]

[a] Centro de Química Estrutural, Institute of Molecular Sciences and Departamento de Química e Bioquímica, Faculdade de Ciências, Universidade de Lisboa, Campo Grande, 1749-016 Lisboa, Portugal
[b] Universidade da Coruña, Grupo NanoToxGen, Centro Interdisciplinar de Química y Biología (CICA), Departamento de Química, Facultade de Ciencias, Campus de A Coruña, 15071 A Coruña, Spain
[c] Department of Medical Microbiology, Albert Szent-Györgyi Medical School, University of Szeged, Semmelweis utca 6, H-6725 Szeged, Hungary
[d] MTA-SZTE Lendület Functional Metal Complexes Research Group, Department of Inorganic and Analytical Chemistry, University of Szeged, Dóm tér 7, H-6720 Szeged, Hungary
[e] Centro de Química Estrutural, Institute of Molecular Sciences, Av. Rovisco Pais, 1049-001 Lisboa, Portugal
[f] Departamento de Engenharia Química, Instituto Superior de Engenharia de Lisboa, Instituto Politécnico de Lisboa, Av. Conselheiro Emídio Navarro, 1, 1959-007 Lisboa, Portugal

ARTICLE INFO

Keywords:
Iron(II)-cyclopentadienyl
Metallodrugs
Anticancer
ABCB1
Colon adenocarcinoma
Redox activity

ABSTRACT

Structure-activity studies aiming to understand the role of each coligand in the formulation of new metallodrugs is an important subject. In that frame, six new compounds with general formula $[Fe(\eta^5\text{-}C_5H_5)(dppe)(\mathbf{L})][CF_3SO_3]$ with **L** = benzonitriles (**1**–**4**) or carbon monoxide (**5**) and compound $[Fe(\eta^5\text{-}C_5H_5)(CO)(PPh_3)_2][CF_3SO_3]$ (**6**) were synthesized and compared with three other previously reported compounds $[Fe(\eta^5\text{-}C_5H_5)(CO)(\mathbf{L})(PPh_3)][CF_3SO_3]$. We were particularly interested in assessing the effect of dppe vs. (PPh_3 + CO) for this set of compounds. For that, all compounds were tested against two human colon adenocarcinoma cell lines, Colo205 and the refractile Colo320 (expressing ABCB1, an efflux pump causing multidrug resistance), showing IC_{50} values in the micromolar range. The presence of dppe in the compound's coordination sphere over (PPh_3 + CO) allows for more redox stable compounds showing higher cytotoxicity and selectivity, with improved cytotoxicity towards resistant cells that is not related to the inhibition of ABCB1. Further studies with GSH and H_2O_2 for selected compounds indicated that their antioxidant ability is not probably the main responsible for their cytotoxicity.

1. Introduction

There is a current great interest in developing new anticancer drugs based on iron [1]. Due to its role in several biological processes in the human body, it is considered essentially non-toxic. Besides, iron is cheap and easily available and, as a transition metal centre, it offers the advantage of versatile electronic and structural features, including a range of oxidation states and geometries and allows for different type and number of coordinated ligands [2]. Thus, the search of new anticancer chemotherapeutics able to overcome the limitations associated to platinum-based drugs finds on iron compounds a convenient choice to discover new anticancer agents. The fundamental chemistry related with different types of ligand substitution, metal- and ligand-based redox processes, constitutes an attractive challenge to medicinal chemists for the design of new structures bringing innovation and possibly new mechanisms of action and targets for metal transition based metallodrugs [3–5]. In this frame, the search of new organometallic anticancer drugs is appealing and, in particular, the research on iron complexes as anticancer agents was triggered by the success of the anticancer effects of ferrocifens [6], the ferrocene analogues of the reference antioestrogen tamoxifen [7], the first line therapeutic for patients with hormone-dependent breast cancer. Yet, despite the good prospects for the ferrocifens family, the inconvenience of their poor bioavailability has been delaying their entrance in clinical trials. Indeed,

* Corresponding author.
E-mail address: amvalente@fc.ul.pt (A. Valente).

https://doi.org/10.1016/j.jinorgbio.2023.112386
Received 10 August 2023; Received in revised form 13 September 2023; Accepted 23 September 2023
Available online 26 September 2023

solubility limitation, commonly found for the lipophilic organometallic compounds, constitutes a current issue to overcome on the development of new organometallic drugs [8,9].

Considering the well-known chemistry based on Fe(η^5-ciclopentadienyl)′ scaffold (FeCp) that has given rise through several decades to a wide variety of structures, from single molecules [10–15] to intricate assemblies, such as for example dendrimers [16], it is surprising that this class of compounds has not attracted the attention of researchers in view to the development of anticancer drugs earlier. Only in the last years a set of results with some relevance [17–28], and mainly centred in two families of compounds, has arisen: 'FeCpP' compounds, where P is a phosphane-based ligand [17,18,21–25], and '$Fe_2Cp_2(CO)_x$' (x = 2, 3) [20,26,27,29]. In general, the compounds show good cytotoxicity in the micromolar range in several cancer cell lines such as human leukaemia (HL-60), ovarian (A2780 and A2780CisR), breast (MCF7) and cervical (HeLa) cancer cells. In the case of diirondicarbonyl complexes, whose advantage may come from the cooperative effect of the two metallic centres, structural features were exploited using different bridging ligands, aminocarbyne, thiocarbyne, allenyl and vinyliminium. The compound with the vinyliminium bridge was the most effective cytotoxic agent on the studied cancer lines [20].

An important contribution to the field of mononuclear structures based on the 'FeCpP' core as cytotoxic agents has been the pioneer work developed by our research group [30]. In 2013 we disclosed the first family of compounds, namely [FeCp(dppe)(imidazole-based)][CF_3SO_3] (dppe = ethylenebis(diphenylphosphane)), where the effect of the imidazole pending arm on the activity of the compounds was studied [18]. All complexes revealed IC_{50} values in the micromolar range, being 3.5- to 7-times more cytotoxic than cisplatin; for example, compound with 1-butylimidazole showed values of 0.22, 0.13 and 2.10 μM against the ovarian A2780, breast MCF7 and cervical HeLa human cancer cell lines, respectively [18].

Other authors published in 2015 four 'FeCpP' based compounds presenting carbohydrates ligands functionalized with nitrile groups with IC_{50} values also in the micromolar range on HCT116 colorectal cancer cells [21]. The best 'FeCpP' compound of this family, bearing a glucose derivative, revealed an IC_{50} of 4.08 μM, a close match to the IC_{50} of 5-fluorouracil used as positive control (IC_{50} of 3.80 μM) [21].

In 2021 other 'FeCpP'-based compounds were described, where the main innovation was the introduction of a silver-based anion, namely [FeCp(CO)(κ^2-dppm)][AgI(hfac)(PMe_3)] (dppm = 1,1-bis(diphenylphosphino)methane; hfac = hexafluoroacetylacetato) [22]. This compound showed IC_{50} values of 0.83 and 3.12 μM against MCF7 and MDA-MB-231 breast cancer cells, respectively, with good selectivity indexes. The role of the additional metal (Ag) it is not yet clear regarding the compound's activity since it seems that the Ag-hfac bond is very weak, leading to the formation of [FeCp(CO)(κ^2-dppm)]$^+$[hfac]$^-$. Yet, the compound with the silver containing anion also inhibited the long-term survival and migration of oestrogen receptor positive (MCF-7) [22].

Systematic studies on this topic by our research group in view to understand structure-activity relationships led us to the design and synthesis of several families of 'FeCpP'-based complexes. Studies on compounds with the general formula [FeCp(PR_3)$_2$L]^n (L = 4-aminobenzonitrile, n = +1; L = I, n = 0) led us to elect the triphenylphosphane as the best phosphane coligand and the cationic structures as the best ones in terms of cytotoxicity [25]. The lower performance of the neutral [FeCp(PR_3)$_2$I] compounds is in accordance with this observation corroborating that the charge of the complexes must be considered on the design of new iron-anticancer drugs [25]. Also, the use of coligands with different electronic features such as imidazole-based ligands [17,18], quinoline- and pyrazinecarbonitriles [24] or benzonitriles [23,25], revealed a high efficiency against a wide panel of human cancer cells, e.g. ovarian A2780 (cisplatin sensitive), breast MCF7, cervical HeLa, leukaemia (HL-60), breast MDA-MB-231 and colon SW480 cancer cells.

Our most recent studies with compounds from the [FeCp(CO)(PPh_3)(imidazole-based ligand)][CF_3SO_3] family in human colon adenocarcinoma cell lines Colo205 and Colo320 revealed that compounds with 1-benzylimidazole and 1H-1,3-benzodiazole were potent ABCB1 inhibitors.[17] ABCB1 (P-glycoprotein) is one of the most important efflux pumps involved in the mechanisms of cancer multidrug resistance (MDR), showing the importance of these findings.

In the present work, the continuation of our structure-activity studies led to the synthesis of a set of new compounds of general formula [Fe(η^5-C_5H_5)(dppe)(**L**)][CF_3SO_3] with **L** = benzonitriles (**1**–**4**) or carbon monoxide (**5**). In view to get a better understanding on the structure-activity relationships and compare the effect of the coligands on the FeCp′ scaffold, specifically the effect of dppe vs. (PPh_3 + CO), this new set of compounds was enlarged with [Fe(η^5-C_5H_5)(CO)(PPh_3)$_2$][CF_3SO_3] (**6**) and other related three compounds previously reported, [Fe(η^5-C_5H_5)(CO)(**L**)(PPh_3)][CF_3SO_3] (**7**–**9**) [23]. The choice of amino and hydroxy-based benzonitriles was based on the possibility of further functionalization with relevant biomolecules through a cleavable linker for future cancer targeting if this new 'FeCp' core molecules show promising activity.

2. Experimental section

2.1. Materials and methods

2.1.1. General considerations

All the reactions were carried out under nitrogen atmosphere while using standard Schlenk techniques. The solvents used were previously dried and freshly distilled under nitrogen atmosphere before use, according to common literature methods. All the reactants and solvents for the redox activity studies were purchased from Sigma-Aldrich in puriss quality. The NMR spectra were recorded on a Brucker Advance 400 spectrometer (Fällanden, Switzerland) (^{1}H, 400 MHz; ^{13}C{^{1}H}-apt, 100.62 MHz; ^{31}P{^{1}H}, 161.97 MHz) at probe temperature. ^{1}H and ^{13}C chemical shifts were reported downfield from the residual solvent peak, whereas the ^{31}P NMR chemical shifts were reported downfield from the external standard 85% H_3PO_4. All resonances were characterized for their chemical shifts (δ), given in parts-per-million (*ppm*), and for their coupling constants (J) expressed in Hertz (*Hz*). Resonance multiplicity is expressed, as follows: singlet (s), doublet (d), triplet (t), multiplet (*m*), and complex (*comp*). All assignments were attributed using HMBC, HMQC, and COSY 2D-RMN techniques. Each sample was prepared under air and at room temperature, while using the most adequate deuterated solvent. The electronic UV–Vis. spectra were recorded in methanol, dimethylsulfoxide (DMSO), PEG400 and PEG400/DMEM (20:80, v:v) solutions (10^{-3} to 10^{-5} M), under air, using 1 cm optical path quartz cells on a Jasco V-660 spectrometer (Elnor, Porto, Portugal) in the range of 200–800 nm. The infrared spectra were recorded in a Shimadzu IRA inffinity-1 FTIR spectrophotometer (Kyoto, Japan) in dry KBr pellets, under air, and at room temperature. Elemental analyses were obtained at Laboratório de Análises, Instituto Superior Técnico, using a Fisons Instruments EA1108 system (Fison Instruments Ltd., Glasgow, UK). Data acquisition, integration, and handling were performed using a PC with the software package EAGER-200 (Carlo Erba Instruments).

2.2. Synthesis

The starting materials [Fe(η^5-C_5H_5)(dppe)I] and [Fe(η^5-C_5H_5)(PPh_3)(CO)I] were prepared following literature procedures [,31,32]. [Fe(η^5-C_5H_5)(CO)$_2$I], was prepared from the commercially available dimer [Fe(η^5-C_5H_5)CO)$_2$]$_2$ following the literature procedure [33].

2.2.1. Synthesis of new complexes with the [Fe(η^5-C_5H_5)(dppe)(L)]$^+$ core

General procedure for the synthesis of [Fe(η^5-C_5H_5)(dppe)(L)][CF_3SO_3], were **L** =.

(**1**) 4-hydroxybenzonitrile; (**2**) 4-aminobenzonitrile; (**3**) 4-

hydroxymethylbenzonitrile; (**4**) 4-aminomethylbenzonitrile.

To a stirred and degassed solution of [Fe(η^5-C_5H_5)(dppe)I] (0.46 mmol) in dry acetone (30 mL), $AgCF_3SO_3$ (0.60 mmol) the respective benzonitriles (0.46 mmol) were added. The reaction was followed by NMR for 24 h at room temperature. After a few hours, it was possible to observe the colour solution changing from dark grey to red. The solution was separated by cannula-filtration and the solvent was evaporated under vacuum. The product was purified by neutral alumina column chromatography, always using a mixture of acetone/*n*-hexane with different proportions adequate to each product. After the column, the product was purified by recrystallization from acetone/*n*-hexane.

2.2.2. Complex 1, [Fe(η^5-C_5H_5)(dppe)(NC-Ph-OH)][CF_3SO_3]

Yield: 78%. Red crystalline powder. Eluent for column chromatography: Acetone/*n*-hexane (1:2).

^{1}H NMR [$(CD_3)_2CO$, Me_4Si, δ/ppm]: 9.71 (s, 1, OH); 8.12 (comp, 4, H_{para}-dppe); 7.65–7.48 (comp, 16, H_{ortho} + H_{meta}-dppe); 6.69 (d, 2, J_{HH} = 8.68, H4); 6.50 (d, 2, J_{HH} = 8.77, H3); 4.63 (s, 5, η^5-C_5H_5); 2.78–2.60 (comp, 4, CH_2-dppe). ^{13}C{^1H}-apt NMR [$(CD_3)_2CO$, Me_4Si, δ/ppm]: 162.76 (C1); 138.12 (C_{ipso}); 135.56 (C2); 134.90 (C3); 134.00 (t,$^4J_{CP}$ = 4.67, C_{para}-dppe); 132.39 (d,$^3J_{CP}$ = 4.77, C1); 129.98 (comp, C_{ortho}-dppe); 116.78 (C4); 102.77 (C5); 80.36 (η^5-C_5H_5); 28.45 (CH_2-dppe). ^{31}P{^1H} NMR [$(CD_3)_2CO$, H_3PO_4, δ/ppm]: 97.35. FTIR [KBr cm^{-1}]: υ (O—H) 3440; υ(C—H aromatics) 3200–2900; υ(N≡C) 2218; υ($CF_3SO_3^-$) 1260, 1160, 1030. UV–Vis in PEG400, λ_{max}/nm[ε/M^{-1} cm^{-1}]:235 (25100); 256 (24350); 275 (Sh); 352 (13500); 376 (Sh); 474 (330). UV–Vis in MeOH, λ_{max}/nm[ε/M^{-1} cm^{-1}]: 274 (Sh); 310 (8367); 369 (Sh); 458 (569). HR-ESI-MS (+, *m/z*) Calc for [1]$^+$: 638.15. Found: 637.67.

2.2.3. Complex 2, [Fe(η^5-C_5H_5)(dppe)(NC-Ph-NH_2)][CF_3SO_3]

Yield: 57%. Red crystalline powder. Eluent for column chromatography: Acetone/*n*-hexane (1:3).

^{1}H NMR [$(CD_3)_2CO$, Me_4Si, δ/ppm]: 8.09 (comp, 4, H_{para}-dppe); 7.65–7.46 (comp, 16, H_{ortho} + H_{meta}-dppe); 6.43 (d, 2, J_{HH} = 8.62, H4); 6.28 (d, 2, J_{HH} = 8.70, H3); 5.73(s, 2, -NH_2); 4.59 (s, 5, η^5-C_5H_5); 2.80–2.49 (comp, 4, CH_2-dppe). ^{13}C{^1H}-apt NMR [$(CD_3)_2CO$, Me_4Si, δ/ppm]: 154.04 (C1); 138.08 ($^1J_{HH}$ = 40, C_{ipso}); 137.07 (C2); 134.33 (C3); 134.04 (t,$^4J_{CP}$ = 4.77, C_{para}-dppe); 132.40 (d,$^3J_{CP}$ = 4.79, C1); 129.98 (comp, C_{ortho}-dppe); 113.99 (C4); 97.62 (C5); 80.10 (η^5-C_5H_5); 28.40 (CH_2-dppe). ^{31}P{^1H} NMR [$(CD_3)_2CO$, H_3PO_4, δ/ppm]: 97.51. FTIR [KBr cm^{-1}]: υ(N—H) 3477–3371; υ(C—H aromatics) 3200–2900; υ(N≡C) 2212; υ($CF_3SO_3^-$) 1260, 1150, 1029. UV–Vis in PEG400, λ_{max}/nm [ε/M^{-1} cm^{-1}]:2 38 (19880); 256 (24350); 279 (20840); 325 (21115); 375 (Sh); 473 (604). UV–Vis in MeOH, λ_{max}/nm[ε/M^{-1} cm^{-1}]: 278 (18660); 322 (1650); 368 (Sh); 506 (Sh). HR-ESI-MS (+, *m/z*) Calc for [2]$^+$: 637.16. Found: 636.70. Elemental analysis (%) Calc. for $C_{39}H_{35}F_3FeN_2O_3P_2S$. C 59.6; H 4.5; N 3.6; S 4.1; Found: C 59.7; H 4.9; N 3.3; S 4.0;

2.2.4. Complex 3, [Fe(η^5-C_5H_5)(dppe)(NC-Ph-CH_2OH)][CF_3SO_3]

Yield: 63%. Red crystalline powder. Eluent for column chromatography: Acetone/*n*-hexane (1:1).

^{1}H NMR [$(CD_3)_2CO$, Me_4Si, δ/ppm]: 8.10 (comp, 4, H_{para}-dppe); 7.64–7.47 (comp, 16, H_{ortho} + H_{meta}-dppe); 7.67 (d, 2, J_{HH} = 7.67, H4); 6.61 (d, 2, J_{HH} = 7.62, H3); 4.81 (s, 2, CH_2OH); 4.68 (s, 5, η^5-C_5H_5); 2.85–2.55 (comp, 4, CH_2-dppe). ^{13}C{^1H}-apt NMR [$(CD_3)_2CO$, Me_4Si, δ/ppm]: 155.27(C1); **149.43 (C2)***; 134.01 (C_{para}-dppe); 132.29 (C4); 131.65 + 131.25 + 129.98 (C_{ortho} + C_{meta}-dppe); 127.07 (C3); **109.81 (C5)***; 80.60 (η^5-C_5H_5); 63.61 (C6). ^{31}P{^1H} NMR [$(CD_3)_2CO$, H_3PO_4, δ/ppm]: 97.17. FTIR [KBr cm^{-1}]: υ(O—H) 3446; υ(C—H aromatics) 3200–3000; υ(C—H aliphatics) 3000–2800; υ(N≡C) 2220; υ($CF_3SO_3^-$) 1263, 1153, 1029 UV–Vis in PEG400, λ_{max}/nm[ε/M^{-1} cm^{-1}]:237 (29000); 250 (Sh); 269 (Sh); 337(6350);396 (3545); 493 (Sh). UV–Vis in MeOH, λ_{max}/nm[ε/M^{-1} cm^{-1}]: 274 (Sh); 335 (5658); 389 (Sh); 505 (Sh). HR-ESI-MS(+, *m/z*) Calc for [**3**]$^+$: 652.16. Found: 651.63. *Only identified through interactions in 2D spectra.

2.2.5. Complex 4, [Fe(η^5-C_5H_5)(dppe)(NC-Ph-CH_2NH_2)][CF_3SO_3]

Yield: 32%. Red crystalline powder. Eluent for column chromatography: Acetone/*n*-hexane (1:2).

^{1}H NMR [$(CD_3)_2CO$, Me_4Si, δ/ppm]: 8.11 (comp, 4, H_{para}-dppe); 7.82 (s, 2, NH_2); 7.64–7.47 (comp, 16, H_{ortho} + H_{meta}-dppe); 7.30 (d, 2, H4); 6.61 (d, 2, J_{HH} = 8 Hz, H3); 4.43 (s, 2,-CH_2NH_2); 4.66 (s, 5, η^5-C_5H_5); 2.81–2.65 (comp, 4, CH_2-dppe). ^{13}C{^1H}-apt NMR [$(CD_3)_2CO$, Me_4Si, δ/ppm]: 154.04 (C1); 138.08 ($^1J_{HH}$ = 40, C_{ipso}); 137.07 (C2); 134.33 (C3); 134.04 (t,$^4J_{CP}$ = 4.77, C_{para}-dppe); 132.40 (d,$^3J_{CP}$ = 4.79, C1); 129.98 (comp, C_{ortho}-dppe); 113.99 (C4); 97.62 (C5); 80.10 (η^5-C_5H_5); 28.40 (CH_2-dppe). ^{31}P{^1H} NMR [$(CD_3)_2CO$, H_3PO_4, δ/ppm]: 97.17. FTIR [KBr cm^{-1}]: υ(N—H aromatics) 3464; υ(C—H aromatics) 3055; υ (N≡C) 2237; υ(C≡O) 1980; υ($CF_3SO_3^-$) 1257, 1172, 1029. UV–Vis in PEG400, λ_{max}/nm[ε/M^{-1} cm^{-1}]: 236 (28850); 265 (Sh); 341 (6030); 397 (Sh); 476 (Sh). UV–Vis in MeOH, λ_{max}/nm[ε/M^{-1} cm^{-1}]: 275 (Sh); 343 (4662); 392 (Sh); 506 (Sh). HR-ESI-MS (+, *m/z*) Calc for [**4**]$^+$: 651.18. Found: 650.70.

2.2.6. Synthesis of complex 5, [Fe(η^5-C_5H_5)(dppe)(CO)][CF_3SO_3]

To a stirred and degassed solution of [Fe(η^5-C_5H_5)(CO)$_2$I] (1.9 mmol) in dry acetone (40 mL), $NaBPh_4$ (2.5 mmol) and dppe (2.3 mmol) were added. The reaction proceeded at room temperature for 24 h (its evolution was followed by ^{1}H NMR). After 30 min it was already possible to see the colour solution change from black to yellow. The precipitates were separated by cannula-filtration and the solvent was evaporated under vacuum. The product, [Fe(η^5-C_5H_5)(CO)(dppe)][BPh_4], was purified by recrystallization from acetone/*n*-hexane. After purification, it was dissolved (0.30 mmol) in dry dichloromethane (20 mL), and $AgCF_3SO_3$ (0.36 mmol) was added. The reaction stayed under stirring at room temperature for 1 h. The solution was separated by cannula-filtration and the solvent was evaporated under vacuum. The product was purified by neutral alumina column chromatography using a mixture of acetone/*n*-hexane (1:2) as eluent. It was possible to obtain crystals adequate for single crystal X-ray diffraction by slow diffusion recrystallization in acetone/*n*-hexane.

Yield: 79%. Yellow crystals. Eluent for column chromatography: Acetone/*n*-hexane (1:2).

^{1}H NMR [$(CD_3)_2CO$, Me_4Si, δ/ppm]: 7.92 (m, 4H, H_{meta2}-dppe); 7.66–7.50 (comp, 12H, H_{ortho1} + H_{para1} + H_{ortho2} + H_{para2}-dppe); 7.47 (m, 4H, H_{meta1}-dppe); 4.66 (t, J_{HH} = 1.41, 5H, η^5-C_5H_5); 3.08 (comp, 2H, CH_2-dppe$_1$); 2.93 (comp, 2H, CH_2-dppe$_2$). ^{13}C{^1H}-apt NMR [$(CD_3)_2CO$, Me_4Si, δ/ppm]: 215.20 (d,$^2J_{CP}$ = 26.66, C≡O); 136.65 (s, Cγ_1-dppe); 134.18 (s, Cγ_2-dppe); 133.61 (t,$^3J_{CP}$ = 5.01, C_{meta1}-dppe); 132.53 (s, C_{para1}-dppe); 132.34 (t,$^3J_{CP}$ = 4.86, C_{meta2}-dppe); 132.08 (s, C_{para2}-dppe); 130.27 (t,$^3J_{CP}$ = 5.15, C_{ortho2}-dppe); 130.10 (t,$^3J_{CP}$ = 5.27, C_{ortho1}-dppe); 85.96 (s, η^5-C_5H_5); 29.62 (comp, CH_2-dppe). ^{31}P{^1H} NMR [$(CD_3)_2CO$, H_3PO_4, δ/ppm]: 92.96. FTIR [KBr cm^{-1}]: υ(C—H aromatics) 3111, 3057, 2975, 2904; υ(C≡O) 1971; υ($CF_3SO_3^-$) 1269, 1149, 1032. UV–Vis in DMSO, λ_{max}/nm[ε/M^{-1} cm^{-1}]: 275 (Sh); 316 (*Sh*); 366 (997); 395 (Sh); 440 (*Sh*). UV–Vis in PEG400, λ_{max}/nm [ε/M^{-1} cm^{-1}]: 252 (23552); 275 (Sh); 317 (7000); 374 (4700). ESI-MS (+, *m/z*) Calc for [**5**]$^+$: 547.10. Found: 547.10. Elemental analysis (%) Calc. for $C_{33}H_{29}F_3FeO_4P_2S$: C 56.9; H 4.1; S 4.6; Found: C 56.7; H 4.3; S 4.0.

2.2.7. Synthesis of complex 6, [Fe(η^5-C_5H_5)(CO)(PPh_3)$_2$][CF_3SO_3]

To a stirred and degassed solution of [Fe(η^5-C_5H_5)(CO)(PPh_3)I] (0.4 mmol) in dry dichloromethane (25 mL), $AgCF_3SO_3$ (0.4 mmol) was added. The reaction stayed under stirring at room temperature for 2 h. After a few minutes, it was possible to observe the colour solution changing from dark grey to red. The solution was separated by cannula-filtration to another Schlenk containing the PPh_3 (1.2 mmol) and the reaction proceeded for 24 h at room temperature. The solution was separated by cannula-filtration and the solvent was evaporated under vacuum. The product was purified by neutral alumina column

chromatography, using a mixture of acetone/*n*-hexane (3:1) as eluent. It was possible to obtain crystals adequate for single crystal X-ray diffraction by slow diffusion recrystallization in acetone/*n*-hexane.

Yield: 65%. Red crystals. Eluent for column chromatography: Acetone/*n*-hexane (3:1).

^{1}H NMR [$(CD_3)_2CO$, Me_4Si, δ/ppm]: 7.75 (t,$^{4}J_{CP}$ = 7.75, 6H, H_{para}-PPh_3); 7.41 (t,$^{2}J_{CP}$ = 7.41, 12H, H_{ortho}-PPh_3); 7.30 (m, 12H, H_{meta}-PPh_3); 4.66 (t,$^{2}J_{CP}$ = 1.71, 5H, η^5-C_5H_5).

^{13}C{^{1}H}-apt NMR [$(CD_3)_2CO$, Me_4Si, δ/ppm]: 220.06 (t,$^{2}J_{CP}$ = 28.00, C≡O); 134.67 (d,$^{1}J_{CP}$ = 45.62, Cγ-PPh_3); 134.03 (t,$^{3}J_{CP}$ = 4.78, C_{meta}-PPh_3); 131.85 (s, C_{para}-PPh_3); 129.78 (t,$^{3}J_{CP}$ = 4.97, C_{ortho1}-PPh_3); 86.62 (s, η^5-C_5H_5); 29.62 (comp, CH_2-dppe). ^{31}P{^{1}H} NMR [$(CD_3)_2CO$, H_3PO_4, δ/ppm]: 57.54. FTIR [KBr cm^{-1}]: υ(C—H aromatics) 3111, 3057; υ(C≡O) 1965; υ($CF_3SO_3^-$) 1273, 1143, 1031. UV–Vis in DMSO, λ_{max}/nm[ε/M^{-1} cm^{-1}]: 278 (Sh); 345 (*Sh*); 387 (1306); 493 (*Sh*). UV–Vis in PEG400, λ_{max}/nm[ε/M^{-1} cm^{-1}]: 250 (28675); 276 (29356); 306 (Sh); 339 (Sh); 396 (2900); 500 (478). ESI-MS (+, *m/z*) Calc for [**6**]$^{+}$: 673.15. Found: 673.60. Elemental analysis (%) Calc. for $C_{43}H_{35}F_3FeO_4P_2S$: C 62.7; H 4.3; S 3.9; Found: C 62.7; H 4.6; S 4.0.

2.3. Electrochemical studies

Cyclic voltammograms were acquired using an EGG Princeton Applied Research Potentiostat/Galvanostat Model 273 A, equipped with Electrochemical PowerSuite v2.51 software for electrochemical analysis. The measurements were run in anhydrous acetonitrile (ACN) with tetrabutylammonium hexafluorophosphate ($TBAPF_6$, 0.1 M) as the supporting electrolyte.

For the experimental setup, a homemade electrochemical cell with a three-electrode configuration was used. The working electrode consisted of a platinum disk (1.0 mm in diameter) probed by a Luggin capillary. A silver-wire pseudo-reference electrode and a platinum wire auxiliary electrode completed the setup. The cyclic voltammograms were recorded over a range of scan rates, specifically from 0.02 to 1.0 V.s^{-1}. All experiments were performed at room temperature under a nitrogen atmosphere. The measured potentials were referenced to the ferrocene/ferrocenium redox couple as an internal standard and reported relative to the saturated calomel electrode (SCE). Under the experimental conditions the potential for ferrocene/ferrocenium redox couple is $E_{1/2}$ = +0.40 V vs SCE. To ensure the quality of the solvents used, reagent-grade materials were dried, purified using standard procedures, and distilled under a nitrogen atmosphere prior to their use in the experiments.

2.4. X-ray crystal structure determination

Three-dimensional X-ray data were collected on a Bruker Kappa Apex-II CCD diffractometer at low temperature for compounds **1**, **5** and **6** by the ϕ-ω scan method. Reflections were measured from a hemisphere of data collected from frames, each of them covering 0.3° in ω. A total of 45,237 for **1**, 75,281 for **5** and 52,897 for **6** reflections measured were corrected for Lorentz and polarization effects and for absorption by multi-scan methods based on symmetry-equivalent and repeated reflections. Of the total, 7845 for **1**, 6553 for **5** and 7486 for **6** independent reflections exceeded the significance level ($|F|/\sigma|F|$) > 4.0. After data collection, an multi-scan absorption correction (SADABS) [34] was applied in each case. The structures of the compounds were solved by direct methods and refined by full matrix least-squares on F^2 data using Olex2 [35,36]. SHELX suite of programs were used for drawing the structures [37]. Hydrogen atoms were included in calculation position and refined in the riding mode. Refinements were done with allowance for thermal anisotropy of all non-hydrogen atoms. A final difference Fourier map showed no residual electronic density: 0.35 and − 0.23 e.Å^{-3} for **1** and 0.55 and − 0.52 e.Å^{-3} for **5**. The final difference Fourier map showed a residual electronic density: 1.94 and − 0.77 e.Å^{-3} for **9**, next to the acetone molecule due a disorder, which couldn't be refined. Weighting schemes of $w = 1/[\sigma^2(F_o^2) + (0.031264\ P)^2 + 0.249029\ P]$ for **1**, $1/[\sigma^2(F_o^2) + (0.023288\ P)^2 + 2.324141\ P]$ for **5** and $1/[\sigma^2(F_o^2) + (0.0542\ P)^2 + 3.060465\ P]$ for **9**, where $P = (|F_o|^2 + 2|F_c|^2)/3$, were used in the latter stages of refinement. Further details of the crystal structure determination are given in **Table S1.** CCDC 2264799-2264801contain the supplementary crystallographic data for the structures reported in this paper. These data can be obtained free of charge via http://www.ccdc.cam.ac.uk/conts/retrieving.html, or from the Cambridge Crystallographic Data Centre, 12 Union Road, Cambridge CB2 1EZ, UK; fax: (+44) 1223 336,033; or e-mail: deposit@ccdc.cam.ac.uk. Supplementary data associated with this article can be found, in the online version, at doi: $$$$$.

2.5. Stability studies

Stability studies were carried out in DMSO, PEG400 and PEG400/DMEM (20:80; *v*/v) by UV–Vis spectroscopy in solutions of compounds **1**–**6** with concentrations between 10^{-4}–10^{-5} M. Their electronic spectra were recorded in the range allowed by the solvent mixture at set time intervals. Samples were stored at room temperature and protected from light between measurements. The variation percentage between measurements were calculated by the following expression:

$$\%variation = \frac{Abs(\lambda, t_{mix}) - Abs(\lambda, t_{mix} + n)}{Abs(t_{mix})} \times 100$$

Where Abs is the absorbance, λ is the wavelength of the measure, t_{mix} is the time at which the first measurement is performed after the solubilization of the compound and t_{mix} + n is the time *n* at which the measure of performed.

The stability of compounds **1**–**4** was also performed by ^{1}H NMR in dimethylsulfoxide-d6.

2.6. Cell cultures

The human colon adenocarcinoma cell lines, the Colo 205 (ATCC-CCL-222) doxorubicin-sensitive and Colo 320/MDR-LRP (ATCC-CCL-220.1) resistant to doxorubicin expressing ABCB1, were purchased from LGC Promochem (Teddington, UK). The cells were cultured in RPMI-1640 medium supplemented with 10% heat-inactivated fetal bovine serum (FBS), 2 mM L-glutamine, 1 mM Na-pyruvate, 10 mM HEPES, nystatin and a penicillin-streptomycin mixture. The MRC-5 (ATCC CCL-171) human embryonic lung fibroblast cell line (LGC Promochem) was cultured in EMEM medium, supplemented with 1% non-essential amino acid (NEAA) mixture, 10% heat-inactivated FBS, 2 mM L-glutamine, 1 mM Na-pyruvate, nystatin, and a penicillin-streptomycin mixture. The cell lines were incubated in a humidified atmosphere (5% CO_2, 95% air) at 37 °C.

2.7. Compounds dilution and storage

Compounds were dissolved in PEG400 as 10 mM solutions. Aliquots were prepared and stored at −20 °C and protected from light. PEG400 percentage in the cell-based assays did not exceed 2%, concentration at which no toxicity is observed.

2.8. Assay for cytotoxic effect

Prior to the assay the cells were seeded overnight in 96-well flat-bottomed microtiter plates: 6 × 10^3 of human colonic adenocarcinoma cells in 100 μL of the medium (RPMI-1640) and adherent human embryonic lung fibroblast cell line (6 × 10^3/well) in EMEM. The effects of increasing concentrations of the compounds on cell growth were tested in 96-well flat-bottomed microtiter plates. The two-fold serial dilutions of the tested compounds were made starting with 100 μM. The serial dilutions of the compounds were made in a separate plate starting with 100 μM, and then transferred to the plates containing the adherent

corresponding cell line. Culture plates were incubated at 37 °C for 48 h; at the end of the incubation period, 20 μL of MTT (thiazolyl blue tetrazolium bromide) solution (from a 5 mg/mL stock solution) were added to each well. After incubation at 37 °C for 4 h, 100 μL of sodium dodecyl sulfate (SDS) solution (10% SDS in 0.01 M HCl) were added to each well and the plates were further incubated at 37 °C overnight. Cell growth was determined by measuring the optical density (OD) at 540 nm (ref. 630 nm) with Multiscan EX ELISA reader (Thermo Labsystems, Cheshire, WA, USA). Inhibition of cell growth was expressed as IC_{50} values, defined as the inhibitory dose that reduces the growth of the cells exposed to the tested compounds by 50%. IC_{50} values and the SD of triplicate experiments were calculated by using GraphPad Prism software version 5.00 for Windows with nonlinear regression curve fit (GraphPad Software, San Diego, CA, USA; www.graphpad.com).

2.9. Rhodamine 123 accumulation assay

The cell numbers of the human colon adenocarcinoma cell lines were adjusted to 2×10^6 cells/mL, re-suspended in serum-free RPMI 1640 medium and distributed in 0.5 mL aliquots into Eppendorf centrifuge tubes. The tested compounds were added at 2 or 20 μM concentrations, and the samples were incubated for 10 min at room temperature. Tariquidar was applied as positive control at 0.2 μM. Next, 10 μL (5.2 μM final concentration) of the fluorochrome and ABCB1 substrate rhodamine 123 (Sigma) were added to the samples and the cells were incubated for a further 20 min at 37 °C, washed twice and re-suspended in 1 mL PBS (*phosphate buffered saline*) for analysis. The fluorescence of the cell population was measured with a PartecCyFlow® flow cytometer (Partec, Münster, Germany). The fluorescence activity ratio was calculated as the quotient between FL-1 of treated/untreated resistant Colo 320 cell line over treated/untreated sensitive Colo 205 cell line according to the following equation:

$$\mathrm{FAR} = \frac{\mathrm{Colo320}_{\mathrm{treated}}/\mathrm{Colo320}_{\mathrm{control}}}{\mathrm{Colo205}_{\mathrm{treated}}/\mathrm{Colo205}_{\mathrm{control}}}$$

The resulting histograms were evaluated regarding mean fluorescence intensity (FL-1), standard deviation, both forward scatter count (FSC) and side scatter count (SSC) parameters of 20,000 individual cells belonging to the total and the gated populations.

2.10. Stability and reactivity of complexes 1 and 2 in ethanol and in DMSO/H_2O solution

UV–visible (UV–vis) spectra of complex **1** and **2** were recorded in ethanol (prior to the DPPH assay) and in 30% (*v*/v) DMSO/H_2O solvent mixture at pH 7.4 (prior to the H_2O_2 and GSH assay) using 30–50 μM complex concentrations. The pH was adjusted with 2-[4-(2-hydroxyethyl)piperazin-1-yl]ethanesulfonic acid (HEPES) buffer (20 mM). The spectra were recorded after different waiting time on an Agilent Cary 8454 spectrophotometer at an interval of 200–800 nm. Concentrated H_2O_2 (30%) and 5 mM GSH stock solutions were used to monitor the reactivity of the complexes. The reaction with GSH was followed under anaerobic conditions (O_2 content ≤1 ppm) in a laboratory glove box (GP(Campus), Jacomex) and an Avantes spectrophotometer was used (model AvaLight-DHc light source equipped with an AvaSpec-UL2048XL-EVO).

2.11. DPPH free radical scavenging assay

The DPPH free radical scavenging capacity of complexes **1** and **2** was determined at 25.0 ± 0.1 °C on an Agilent Cary 3500 spectrophotometer in ethanol. The stock solutions of DPPH, trolox and the complexes were freshly prepared. The concentration of DPPH was 40 μM in the final samples and for the investigated compounds it was in the range 0–108 μM. UV–vis spectra were recorded at various time-points (max. 24 h). Trolox was used as the positive control. The percentage of the antioxidant activity (AA) was calculated using the following formula:

$$AA\% = \left(\frac{Absorbance_{negative\ control} - Absorbance_{sample}}{Absorbance_{negative\ control} - Absorbance_{control}}\right) \times 100$$

where $Absorbance_{negative\ control}$ is the absorbance of DPPH, $Absorbance_{sample}$ is the absorbance of the sample solution in the end of the redox reaction (or at the indicated time-point) and $Absorbance_{control}$ is the absorbance obtained after the reaction with trolox at 100% of antioxidant activity. The AA% values were calculated using absorbance values measured at the 515–550 nm. The IC_{50} values, which are the concentrations of compound at which 50% of DPPH is reduced, was calculated according to the following procedure: the antioxidant activity was plotted against the concentration, and the obtained points were fitted with a logistic function using the 'Solver' add-in program of Microsoft Excel; then the IC_{50} value (at which AA% = 50) was calculated with the obtained equation. The DPPH radical scavenging activity of samples was also expressed as trolox equivalent antioxidant capacity (TEAC) [38]. TEAC was calculated as follows: TEAC = IC_{50}(trolox) / IC_{50}(tested compound).

3. Results and discussion

In the present work a family of six new compounds was synthesized. Compounds **1**–**4** were synthesized by halide abstraction from [Fe(η^5-C_5H_5)(dppe)I] using $AgCF_3SO_3$ in the presence of adequate ligands (4-hydroxybenzonitrile (**1**), 4-aminobenzonitrile (**2**), 4-hydroxymethylbenzonitrile (**3**), 4-aminomethylbenzonitrile (**4**)), in acetone with stirring at room temperature for 24 h (Scheme 1A). Additionally, compound **5**, [Fe(η^5-C_5H_5)(CO)(κ^2-dppe)][CF_3SO_3], was synthesized in two stages (Scheme 1B), starting from [Fe(η^5-C_5H_5)(CO)$_2$I] in acetone at room temperature with the coordination of the bidentate dppe ligand in the presence of $NaBPh_4$ originating [Fe(η^5-C_5H_5)(κ^2-dppe)(CO)][BPh_4]. After isolation and purification, the counterion was replaced by reaction with $AgCF_3SO_3$ to obtain the final complex [Fe(η^5-C_5H_5)(CO)(κ^2-dppe)][CF_3SO_3] (**5**). Compound **6**, [Fe(η^5-C_5H_5)(CO)(PPh_3)$_2$][CF_3SO_3], was synthesized using [Fe(η^5-C_5H_5)(CO)(PPh_3)I] as starting material, in dichloromethane at room temperature, using an excess of PPh_3 (Scheme 1C). All compounds were purified by slow diffusion recrystallization and, in some cases, by chromatography in neutral alumina (details in the experimental section). Adequate single crystals for structural determination by X-ray diffraction studies were obtained for compounds **1**, **5** and **6**.

Finally, three other cationic complexes previously reported[23] were included, namely [Fe(η^5-C_5H_5)(CO)(PPh_3)(**L**)][CF_3SO_3] (L = 4-hydroxybenzonitrile (**7**), 4-aminobenzo- nitrile (**8**), 4-hydroxymethylbenzonitrile (**9**)) (Scheme 1D), to complete all the possible combinations of coligands in view to support the main structural features relevant for the cytotoxicity of this family of 'FeCpP' compounds.

3.1. Nuclear magnetic resonance spectroscopy

All complexes were completely characterized by unidimensional (^{1}H, ^{13}C{^1H}-apt, ^{31}P{^1H}) and bidimensional (HMQC, HMBC, COSY) NMR techniques. Yet, there are some signals that are difficult to attribute due to the presence of many peaks in the same region, and in addition, due to the fluxionality revealed by the dppe ligand [39], it is even more difficult to differentiate between all the aromatic dppe carbons in the ^{13}C{^1H}-apt spectra. For the new complexes with dppe ligand **1–4**, the coordination of nitriles is easily confirmed by ^{1}H NMR due to the very significant shielding ($\Delta\delta = -1.1$ ppm, see **Table S1**) of the nitrile H_3 proton (ortho) which reveals a strong π-backdonation from $d_{Fe} \rightarrow \pi^*_{NCR}$. This electronic delocalization agrees with the MLCT bands observed in the electronic spectra of these compounds (Section 3.3). This effect is common to the four complexes as it can be observed in **Table S1**. For these complexes (**1**–**4**), a deshielding on the 'Cp' of ~0.2 ppm was also

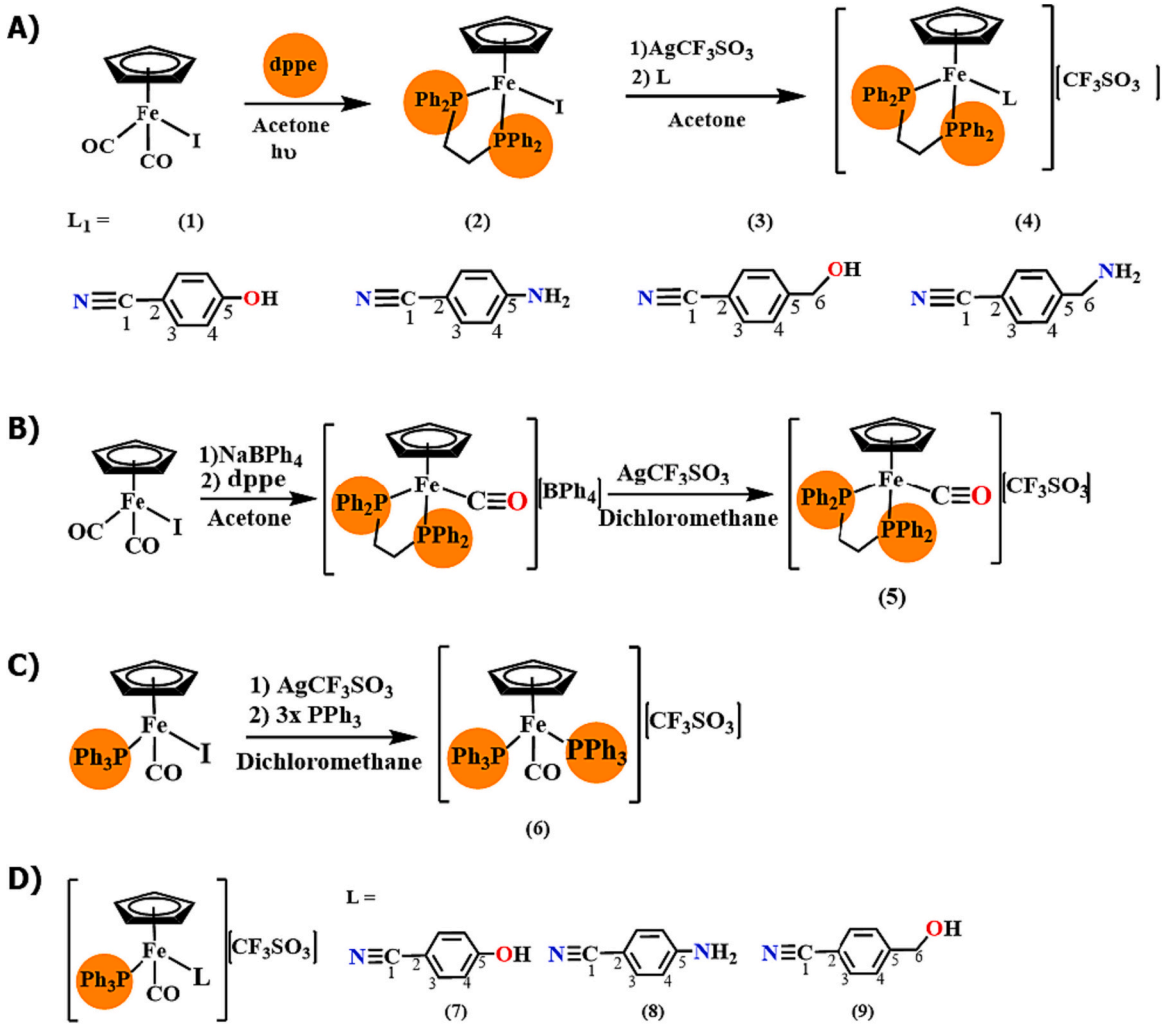

Scheme 1. General scheme for the synthesis of the new cationic complexes of general formula $[Fe(\eta^5\text{-}C_5H_5)(dppe)(\mathbf{L})][CF_3SO_3]$ (**1–5**) (**A** and **B**) and $[Fe(\eta^5\text{-}C_5H_5)(CO)(PPh_3)_2][CF_3SO_3]$ (**C**). In **D)** the previously reported compounds **7–9** with general formula $[Fe(\eta^5\text{-}C_5H_5)(CO)(PPh_3)(\mathbf{L})][CF_3SO_3]$ are presented. The ligands are numbered for NMR purposes.

noticeable. As expected, compound **5** with a CO coligand showed a higher deshielding ($\delta = +0.7$ ppm) on the 'Cp' ligand, due to the nature of this excellent π-acceptor, causing π-backdonation ($d_{Fe} \rightarrow \pi^*_{C\equiv O}$) and withdrawing even more electronic density from the 'Cp' ligand.

The $^{31}P\{^1H\}$ spectra of complexes with dppe ligand are characterized by the presence of a single signal at ~97 ppm for compounds **1**–**4** and at 92 ppm for complex **5**. Complex **6**, $[Fe(\eta^5\text{-}C_5H_5)(CO)(PPh_3)_2][CF_3SO_3]$, presents a sharp singlet at 57 ppm, more shielded than compounds **7**–**9** with a nitrile ligand instead of a second PPh_3.

Detailed spectroscopic data concerning APT-$^{13}C\{^1H\}$ NMR experiments are included in the Experimental Section and are in accordance with the effects discussed.

3.2. Fourier-transform infrared spectroscopy

The solid-state FT-IR spectra (KBr pellets) of the organometallic new iron-cyclopentadienyl compounds (**1**–**6**) show the presence of the typical bands attributed to the characteristic vibrations of the functional groups present in the molecule and are described in the experimental section. Of note, the presence of the υ(N≡C) stretching in complexes **1**–**4** was confirmed at slightly lower values than the free nitriles (−2 to −15 cm^{-1}). These negative shifts are in good agreement with the values found before for other related 'Fe-Cp' compounds and are compatible with the electronic delocalization associated to the MLCT bands (UV–vis spectroscopy; section 3.3), and show an enhanced π-backdonation from the metal d orbitals to the π* orbital of the N≡C group leading to a decreased N≡C bond order [,24,40]. The ν_{CO} of compound **6** can also be observed at 1965 cm^{-1}. Comparing to the previous reported complexes bearing a nitrile ligand (**7**–**9**) instead of the second PPh_3, one can notice an improved π backdonation to CO. The same effect was found for complex **5**, but less pronounced, whereas the υ(CO) vibration appears at 1971 cm^{-1} since dppe is not such a good donor as PPh_3.

3.3. Ultraviolet-visible spectroscopy

The optical absorption spectra of the new complexes (**1–6**) were performed in methanol and PEG400 solutions (10^{-3} and 10^{-5} M). The spectra of all compounds present the same general trend as shown for MeOH in Fig. 1A.

All spectra are characterized by a strong absorption band and/or shoulders below 300 nm attributed to the π → π* intramolecular transitions of aromatic ligands (benzonitriles, dppe and PPh_3), one band between 300 and 340 nm attributed to the electronic transitions that occur in the organometallic fragment $\{Fe(\eta^5\text{-}C_5H_5)\}^+$ by analogy with other related compounds and the spectra obtained by DFT calculations [23] In the 350–430 nm region it is possible to verify the presence of a distinct band for compounds **5** and **6** probably due to MLCT transitions from $d_{Fe} \rightarrow \pi^*_{CO}$. The remaining compounds present on this same region

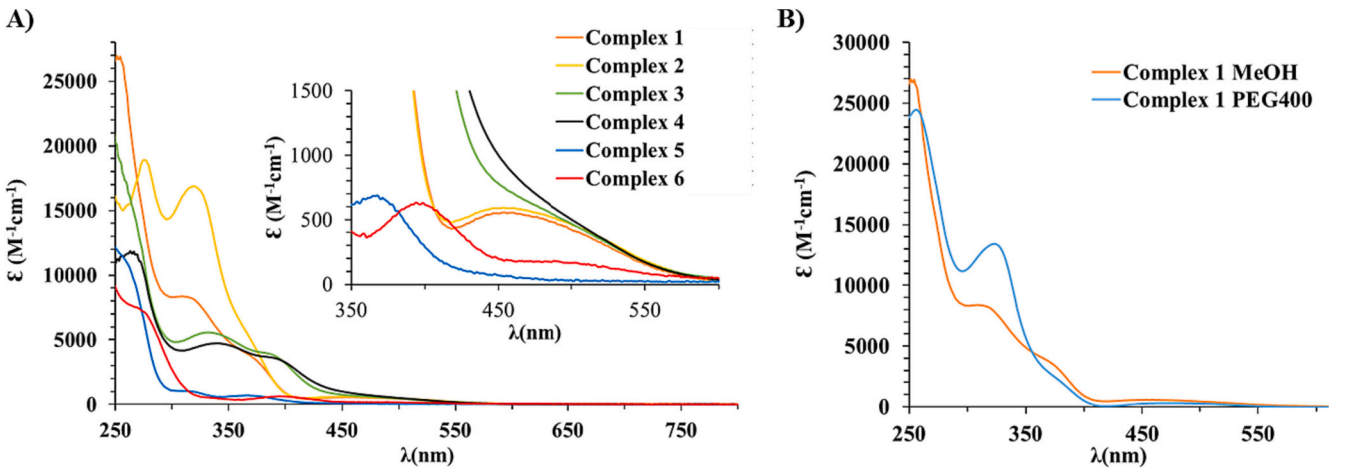

Fig. 1. Electronic spectra of the new compounds **1**–**6** in MeOH solutions (**A**); Solvatochromic study in MeOH and PEG400 for complex **1** (**B**).

broad shoulders which origin can be attributed to MLCT transitions from $d_{Fe} \rightarrow \pi^*_{NCR}$.

The presence of these MLCT bands is corroborated by our NMR and FTIR results discussed in the previous sections. Finally, in the 480–560 nm region there is a broad band for compound **6** of weak intensity characteristic of the d-d transitions occurring in the transition metal centre appearing as shoulders for the other compounds.

Additional UV–visible spectroscopic studies in PEG400 solutions, with different polarity from MeOH, allowed the evaluation of the solvatochromic effect and also the confirmation of the charge transfer character of the observed bands. Indeed, this effect is clearly seen on the electronic spectrum of complex **1** (Fig. 1B), being more noticeable on the $\pi \rightarrow \pi^*$ intramolecular transitions occurring between 300 and 340 nm which appear at higher energy in methanol than in PEG400; the MLCT transitions from $d_{Fe} \rightarrow \pi^*_{NCR}$ become broader and weaker in the PEG400 spectra. This same effect holds for compounds **2–6**.

3.4. Electrochemical studies

To characterize the redox properties of the complexes **1–6**, electrochemical studies were performed by cyclic voltammetry in ACN/$TBAPF_6$ solutions. These studies were also extended to the previously reported compounds **7–9**. Table 1 provides the electrochemical data obtained at room temperature. The iron(II) dppe based family (**1–4**) is generally characterized by the presence of one distinct redox process in the anodic region reversible or quasi-reversible ($E_{1/2}$ in the range + 0.64 − +0.75 V) attributed to the Fe(III)/Fe(II) couple. In some cases, a second irreversible process occurs in the range + 1.30 − +1.64 V. In the cathodic region, one irreversible process was generally observed, probably related with the presence of the nitrile ligands. The typical electrochemical behaviour of the complexes is presented for complex **2** (Fig. 2A).

Table 1
Electrochemical data for compounds **1**–**9** in acetonitrile.

	E_{pa} (V)	E_{pc} (V)	$E_{1/2}$ (V)	$E_{pa} - E_{pc}$ (mV)	I_{pc}/I_{pa}
1	0.74	0.65	0.70	90	1.0
		−1.65			
2	1.64				0.9
	0.68	0.61	0.64	70	
		−1.62			
3	1.45				1.0
	0.81	0.68	0.75	130	
		−1.11			
4	1.30				0.7
	0.80	0.66	0.73	140	
		−1.47			
5	1.57	1.45	1.51	120	0.6
		0.65			
6	1.49				
		- 1.02			
	−1.54	−1.41	- 1.48	130	
7	1.42				
		- 1.12			
		−1.98			
8	1.41				
		- 1.09			
		−1.59			
9	1.45				
		- 1.04			

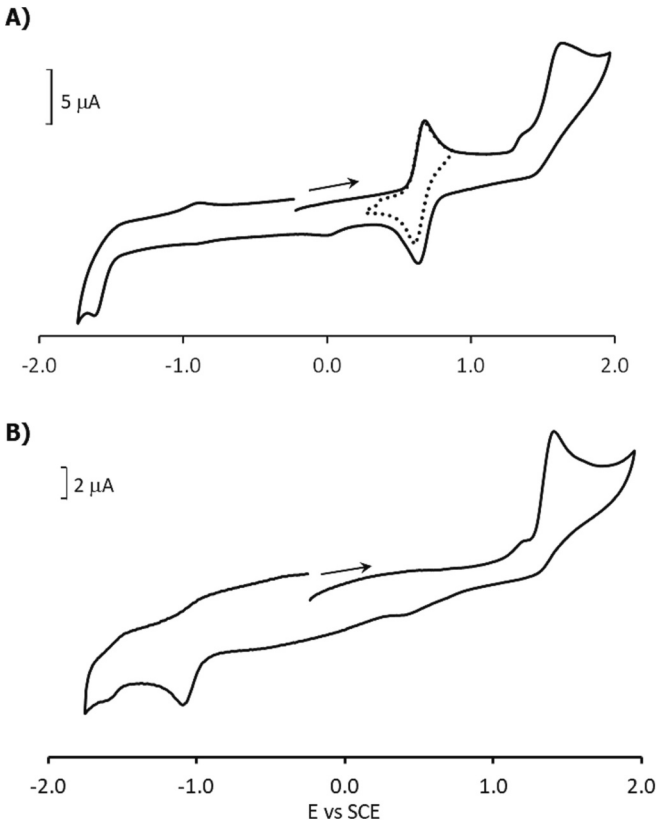

Fig. 2. Cyclic voltammograms of **A)** complex $[Fe(\eta^5\text{-}C_5H_5)(dppe)(NC\text{-}Ph\text{-}NH_2)][CF_3SO_3]$, **2** showing the isolated Fe(III)/Fe(II) process (dashed line) and **B)** complex $[Fe(\eta^5\text{-}C_5H_5)(PPh_3)(CO)(NC\text{-}Ph\text{-}NH_2)][CF_3SO_3]$, **8** in acetonitrile (scan rate = 200 $mV.s^{-1}$).

The trend found for the potentials of the Fe(III)/Fe(II) showed that the electron density of the iron centre is influenced by the presence of the different nitrile ligands and is aligned with the relative donor capacities of the substituents. The NH_2 and OH groups, known for their electron-donating capacity, exhibit lower potentials, with NH_2 showing the lowest value. Moreover, the introduction of a methylene bridge between the aromatic ring and the donor group reduces the electron density at the metal centre, resulting in higher potentials. Replacing the nitrile ligand with a carbonyl group in **5** causes a shift in the potential of the Fe(III)/Fe(II) pair by >800 mV, associated with a more challenging oxidation of the iron(II) centre resulting from the stronger π-backdonation effect to the carbonyl group.

The substitution of the dppe ligand by the pair CO/PPh_3 (compounds **7–9**) leads to significant changes in the redox behaviour of the complexes. The typical electrochemical behaviour of this family is presented for complex **8** (Fig. 2B). All the compounds showed an irreversible oxidation attributed to the Fe(III)/Fe(II) couple. The absence of a cathodic response for this electron transfer process indicates the instability and/or lability of the Fe(III) species formed, likely coupled with a chemical reaction. Moreover, this oxidative process is shifted to higher potentials up to 730 mV. These shifts can be related with a decrease of the electron density on the metal centre due to the π-backdonation competition between the CO and nitrile ligands. It is also evident from Table 1 that for this series the oxidation potentials of the Fe(III)/Fe(II) couple are not significantly affected by the change of the nitrile ligands as for the dppe series. In the cathodic region, one irreversible process was generally observed, probably related with the presence of the phosphane coligand since a similar process is also present in compound **6**.

3.5. Single crystal structures of the compounds 1, 5 and 6

Fig. 3 shows ORTEP representations of the cation complexes **1**, **5** and **6**. Triflate anions, in the three compounds, and one THF molecule in compound **5**, and one acetone molecule in compound **6** complete the asymmetric units. Compound **1** crystallizes in a chiral space group, $P2_1$, while compounds **5** and **6** made so in centrosymmetric space groups (see **Table S2** and **Figs. S26-S28**). Compound **1** presents a unique isomer in the crystal packing. Compounds **5** and **6** contain enantiomer pairs (see **Figs. S29-S31**). A "piano stool" distribution, around of the iron centers, which is formed for Fe-Cp unit and for the dppe ligand in compounds **1** and **5**, and two PPh_3 ligands in compound **6**, 4-hydroxybenzylamine in compound **1** and the CO groups in compounds **5** and **6** were analyzed. Centroid of the π-cloud of cyclopentadienyl moiety to Fe center distances are: 1.7051(1) Å in **1** (ring slippage, 0.012 Å), 1.7105(2) Å in **5** (ring slippage, 0.030 Å) and 1.7337(1) Å in **6** (ring slippage, 0.015 Å). The mean distance from metal center Fe(1) to carbon atoms of the Cp units are: 2.0896(1) Å in **1**, 2.0918(2) Å in **5** and 2.1131(2) Å in **6** (see **Table S3**). The C—O bond lengths, 1.144(2) Å in **5** and 1.152(3) Å in **6**, have a usual value for organometallic compounds [25].

Compound **1** presents interactions by hydrogen bonds between the hydroxy group of 4-hydroxibenzylamine ligand and oxygen atoms of the

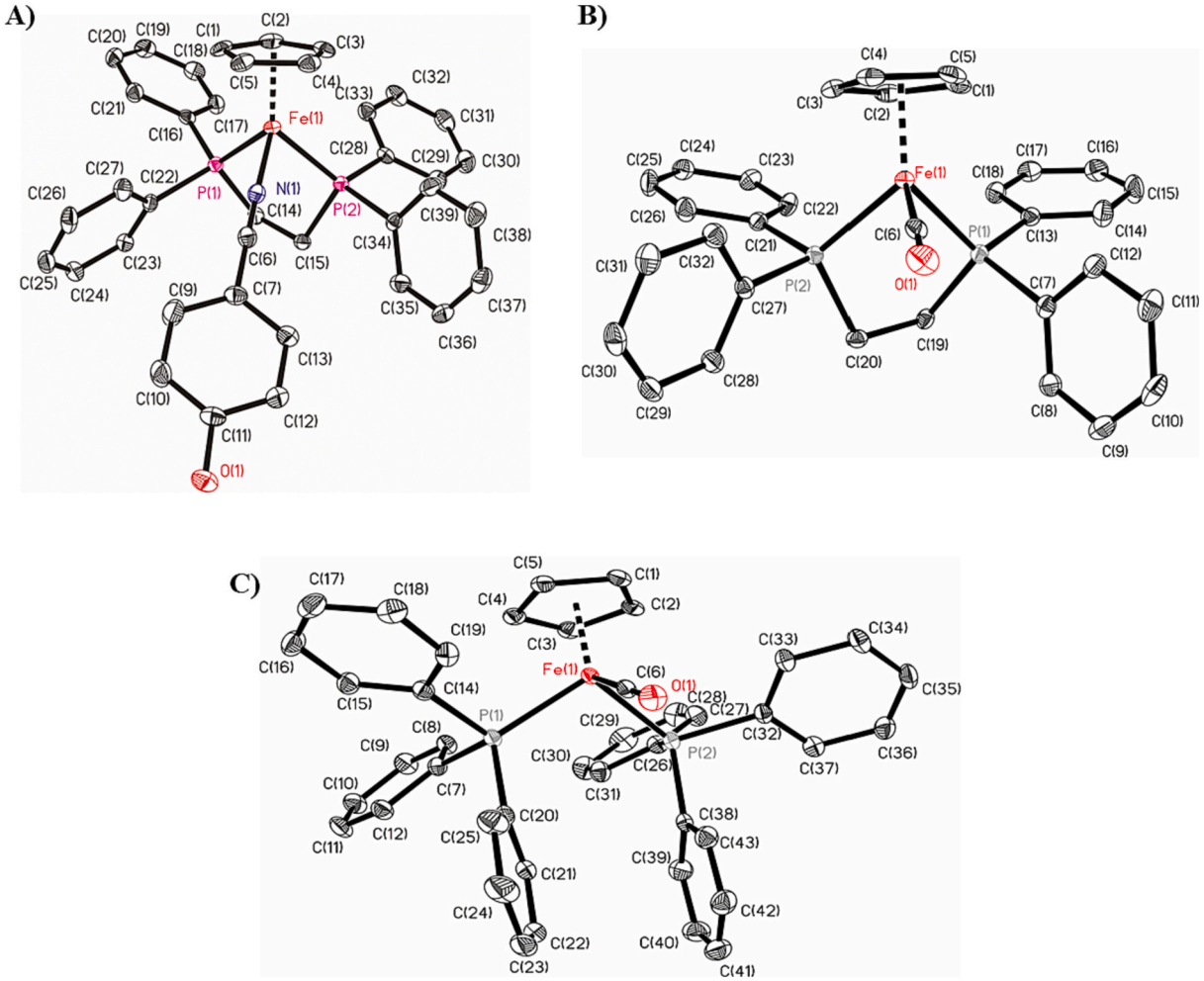

Fig. 3. ORTEP for the cation complex in **A)** compound **1**; **B)** compound **5** and **C)** compound **6**. All the non-hydrogen atoms are presented by their 50% probability ellipsoids. Hydrogen atoms are omitted for clarity.

$(CF_3SO_3)^-$ anions. This hydrogen bond has a distance between donor acceptor atoms of 2.684(2) Å, an angle of 172.6°, and the symmetry transformation used to generate equivalent atoms is x + 1,y,z + 1.

3.6. Chemical reactivity

For the intended application as anticancer agents, it is desirable that the compounds under study are stable in the cellular environment. Since the present compounds are not soluble in water, they need to be solubilized using a co-solvent. DMSO is commonly used as co-solvent for in vitro studies. Accordingly, the stability of these compounds was tested by UV–Vis spectroscopy in this solvent. While complexes **5** and **9** are stable in DMSO, the spectra of compounds **1–4** show a decrease in the bands related to the metallic fragment (> 300 nm) over time suggesting ligand decoordination (**Fig. S32**). NMR studies (^{1}H and ^{31}P{^1H}) in DMSO-d_6 confirmed this assumption (example for complex **1** in Fig. 4) with the appearance of the signals of free dppe and nitriles and the concomitant formation of $[Fe(Cp)(dppe)(DMSO)]^+$ complex. As such, we decided to study the stability in compounds **1**–**6** in PEG400, an hydrophilic polymer, considered one of the most safe co-solvents for preclinical assays [41]. In this solvent, all compounds were quite stable up to 24 h, with absorbance variations of <9% (**Figs. S33-S38**). Stability of the compounds in cell media (DMEM) containing 20% PEG400 was also assessed for a 3 h period (Figs. **S39-S44**). Under these conditions, all the complexes showed adequate stability, allowing their further in vitro studies.

3.7. Biological studies

3.7.1. Cytotoxicity in colon adenocarcinoma cell lines

Colorectal cancer is among the most prevalent type of cancers and is the second cause of cancer death worldwide [42]. Resistance to chemotherapy, mainly for metastatic disease, remains one of the greatest challenges to overcome. In that frame, the activity of the compounds was examined on two colon adenocarcinoma cell lines (Colo205 without ABCB1 expression and Colo320 with ABCB1 expression; one of the main causes of multidrug resistance) and on normal embryonal lung fibroblasts (MRC-5) (Table 2). Except for **6** and **8**, all compounds had strong cytotoxic effect on both cell lines, exhibiting IC_{50} values lower than 10 μM. Five out the nine tested complexes (namely, **2**–**4**, **8** and **9**) show more pronounced activity on the ABCB1 expressing Colo 320 cell line compared to the sensitive Colo205 cell line without ABCB1 expression (RR < 1) [43], thus showing selectivity against resistant cells.

Table 2
IC_{50} values determined at 48 h incubation of iron compounds (**1**–**9**) against Colo205: doxorubicin sensitive human colon adenocarcinoma cell lines, Colo320: doxorubicin resistant human colon adenocarcinoma cell line and MRC5: human embryonic fibroblast cell lines. Selectivity index: ratio of the IC_{50} values obtained on the non-cancerous and the cancer cells. RR: Relative Resistance Ratio = IC_{50} of the resistant Colo320 cell line /IC_{50} of the sensitive Colo205 cell line [43].

Compounds	IC_{50} (μM)			RR	SI	
	Colo205	Colo320	MRC-5		MRC5/ Colo205	MRC5/ Colo320
1	1.80 ± 0.21	6.4 ± 0.3	13.72 ± 1.84	3.56	**7.62**	2.14
2	0.73 ± 0.04	0.68 ± 0.08	8.98 ± 1.46	**0.93**	**12.32**	**13.30**
3	1.81 ± 0.28	1.61 ± 0.23	11.53 ± 4.04	**0.89**	**6.37**	**7.15**
4	4.22 ± 0.64	3.90 ± 0.12	19.32 ± 4.62	**0.92**	4.58	4.96
5	2.69 ± 0.03	12.1 ± 1.2	8.59 ± 1.17	4.52	3.20	0.71
6	1.31 ± 0.17	6.1 ± 0.2	3.20 ± 0.49	4.64	2.44	0.53
7	9.42 ± 2.05	13.39 ± 2.89	11.07 ± 2.09	1.42	1.17	0.83
8	15.06 ± 0.47	9.51 ± 0.39	13.75 ± 1.87	**0.63**	0.91	1.44
9	4.28 ± 0.30	2.66 ± 0.64	8.00 ± 0.57	**0.62**	1.87	3.01
Cisplatin	5.60 ± 0.21	3.84 ± 0.20	2.97 ± 0.11			
Doxorubicin	1.2 ± 0.05	1.75 ± 0.36	1.28 ± 0.19			

Regarding the selectivity towards cancer cells, the IC_{50} values measured on cancer cells were compared with the IC_{50} values on normal MRC-5 cells. Compounds **1**–**3** demonstrated strong selectivity towards Colo205 cells with SI of 7.62, 12.32 and 6.37, respectively. Compounds **4** and **5** exhibited moderate selectivity towards Colo205 cells (SI of 4.58 and 3.2, respectively). In addition, compounds **2** and **3** were strongly selective anticancer agents on Colo320 cells, exhibiting selectivity indices of 13.3 and 7.15, respectively. Moderate selectivity towards

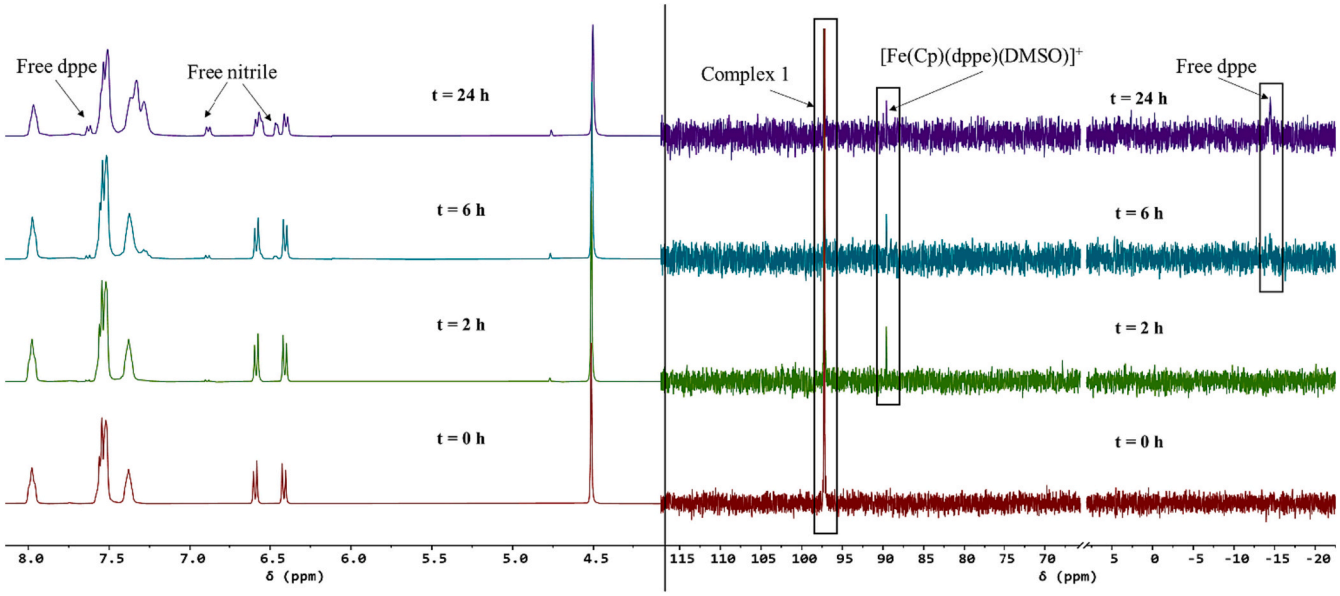

Fig. 4. Stability studies for $[Fe(\eta^5\text{-}C_5H_5)(\kappa^2\text{-dppe})(4\text{-hydroxybenzonitrile})][CF_3SO_3]$ (**1**) in DMSO-d_6 during 24 h: ^{1}H NMR (Left) and ^{31}P{^{1}H} (Right).

Colo320 cells was demonstrated in the presence of **4** and **9**, with SI of 4.96 and 3.01.

Regarding the compound's structure, one can notice that for the compounds bearing the same nitrile (**1** vs. **7**; **2** vs. **8** and **3** vs. **9**), the change from having a dppe ligand instead of (PPh_3 + CO) led to an increase on the cytotoxicity by 2–21 times, depending on the cancer cell. Curiously, for compounds **5** and **6**, without any nitrile, the PPh_3 bearing compound (**6**) is more cytotoxic than the one with dppe (**5**). Yet, these are also the compounds for which the relative resistance ratio is higher, suggesting that the nitrile is important for the overall complex activity. The compounds bearing dppe also afford complexes with the better selectivity indexes.

3.8. ABCB1 inhibition: Rhodamine 123 accumulation assay

The effect of the complexes **1**–**9** on the ABC-transporter ABCB1 (P-glycoprotein, P-gp) efflux pump was monitored via the rhodamine 123 fluorometric accumulation assay. The noncompetitive P-glycoprotein inhibitor, tariquidar, was used as a positive control [44]. Based on this assay none of the present iron compounds could inhibit the ABCB1 MDR efflux protein of Colo320 cells (**Table S4**). We recently disclosed the first Fe(II) organometallic compounds as ABCB1 inhibitors, namely [Fe(η^5-C_5H_5)(CO)(PPh_3)(Imi-R)][CF_3SO_3] (Imi-*R* = 1-benzylimidazole or 1*H*-1,3-benzodiazole) [17]. On that study we concluded that the substituent at the imidazole ring was important for the observed activities. As such, more lipophilic groups could be considered as substituents at the nitrile-based ligand in a future study for the present family of compounds.

3.9. Redox activity of complexes 1 and 2

We selected the most cytotoxic and selective compound **2** and the simplest compound **1**, for further redox activity studies, potentially associated to their biological activity. These two compounds also showed the best redox behaviour on the cyclic voltammetry studies revealing a good stability on the pair Fe(III)/Fe(II) that would allow the formation of oxidized species. Compounds **1** and **2** redox activity was monitored in the presence of physiologically relevant oxidizing (H_2O_2) and reducing (GSH) agents. The tripeptide GSH is not only a powerful reducing agent in the biological systems with significant antioxidant activity, but as a complexing agent since it can also coordinate to metal ions replacing the original ligands or forming mixed-ligand complexes. GSH is found in millimolar concentrations within the cytoplasm and its level is often elevated in cancer cells [45]. As a first step, the complexes were reacted with high excess of GSH at pH 7.4 in 30% (*v*/v) DMSO/H_2O under strictly O_2-free conditions in a laboratory glove box, and time-dependent UV–Vis spectra were recorded (Fig. 5). The presence of DMSO was necessary to provide the adequate solubility. The recorded spectra exhibited minimal changes during the monitored ca. 2–2.5 h, which suggest no redox reaction or ligand-replacement. To further explore the effect of the presence of GSH, ^{1}H NMR spectra were also recorded for complex **2** (Fig. 6). The spectra showed negligible changes of the peaks associated with the ligands coordinated to the metal complex.

Then the effect of H_2O_2 as oxidizing agent on the UV–Vis spectra of these Fe(II) complexes was tested at pH 7.4 (Fig. 7). The spectra showed significant changes upon the addition of H_2O_2, however, without this reagent similar but slower changes were also observed. Comparing the spectra, it can be concluded that complexes **1** and **2** exhibit a gradual oxidation process under aerobic conditions, with the oxidation rate being augmented in the presence of H_2O_2. The oxidation of these Fe(II) complexes may lead to the generation of reactive oxygen species. This particular property enables the complexes to act as antioxidant agents. Therefore, the antioxidant activity of the complexes was tested using the DPPH assay [46].

The direct reaction of complexes **1** and **2** with the DPPH radical was studied by UVVvis spectrophotometry in ethanol using various complex-to-DPPH ratios up to 24 h. Prior to conducting the assay, the stability of the complexes in ethanol was also checked (Fig. 8). The recorded spectra showed slow but clear changes, similarly to the phenomena observed in 30% (v/v) DMSO/H_2O (under aerobic conditions), which has to be taken into account when interpreting the results of the DPPH assay.

Representative UV–Vis spectra are shown for the complexes upon the reaction with DPPH in Fig. 9A,B at their equimolar ratio. In the monitored wavelength range ($\lambda > 400$ nm) the complexes (or their oxidized product) have no contribution to the measured absorbance, thus, the observed spectral changes are solely attributed to the DPPH radical. The spectra at all the applied complex-to-DPPH ratios showed a biphasic feature indicating a complex reaction. It should be also noted that the reaction is relatively slow and at the lower equivalents of the complexes the redox equilibrium could not be reached even after a 24 h period as Fig. 9C represents for complex **2**, where changes in absorbance at the λ_{max} of DPPH (517 nm) in time at the different complex-to-DPPH ratios are compared. Considering all these observations, the quenching of the DPPH radical was computed at a selected time-point (8 h, see Fig. 9D). The free radical scavenging activities are generally indicated as IC_{50} values (the concentration at which the compound reduces 50% of the DPPH radicals present in the reaction mixture). These values were calculated for the data collected at 8 h, and the following IC_{50} values were obtained: complex **1**: 40 μM, complex **2**: 63 μM. They can be compared to that of the reference compound trolox under the same condition: 10.5 μM, giving trolox equivalent antioxidant capacity (TEAC) values as 0.26 and 0.17 for complex **1** and **2**, respectively. The

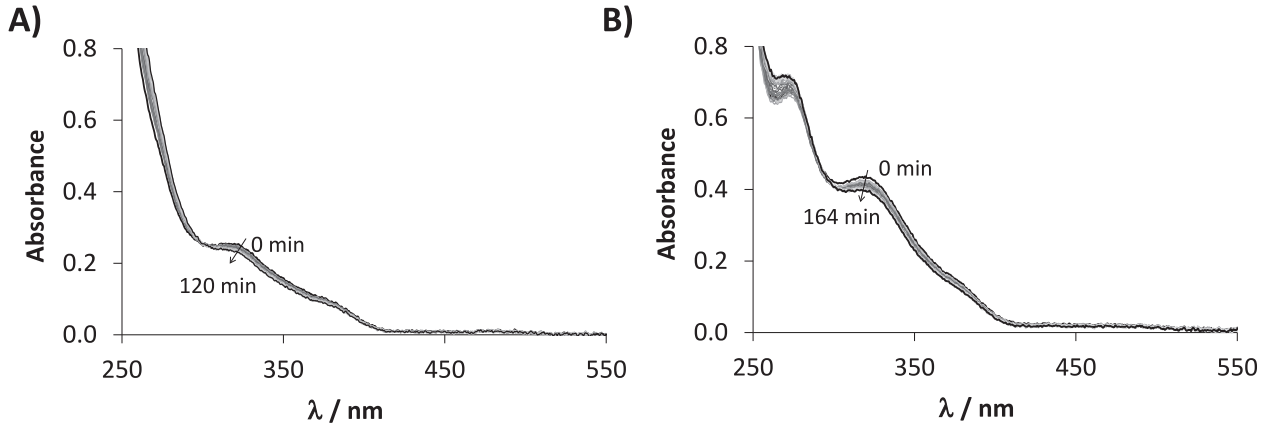

Fig. 5. Time-dependent changes of the UV–visible spectra of complex **1** (15 μM) with GSH (3 mM) (**A**), and complex **2** (25 μM) with GSH (1.5 mM) (**B**) at pH 7.4. (20 mM HEPES; ℓ = 1 cm; T = 25 °C; I = 0.10 M KCl).

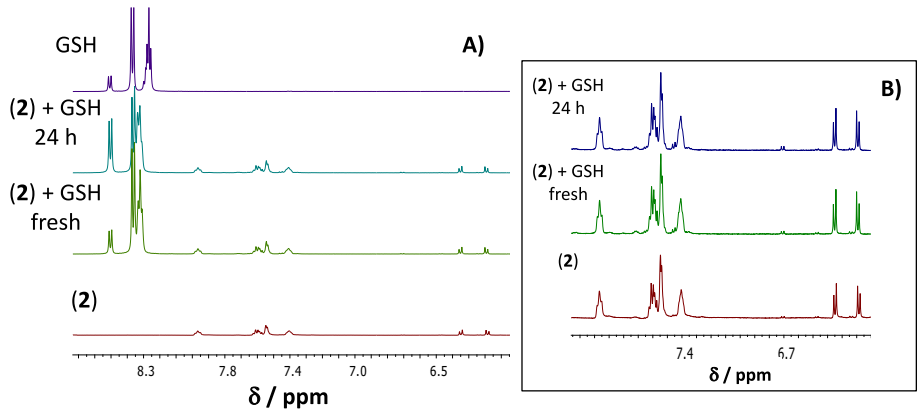

Fig. 6. ^{1}H NMR spectrum of complex **2**, GSH and their mixtures in the down-field range recorded freshly and after 24 h at pH 7.4 (20 mM phosphate buffer) in 30% (*v*/v) d_6-DMSO/H_2O (**A**). Enlargement of selected spectra (**B**). (c_{GSH} = 20 mM; $c_{complex}$ = 0.39 mM; T = 25 °C).

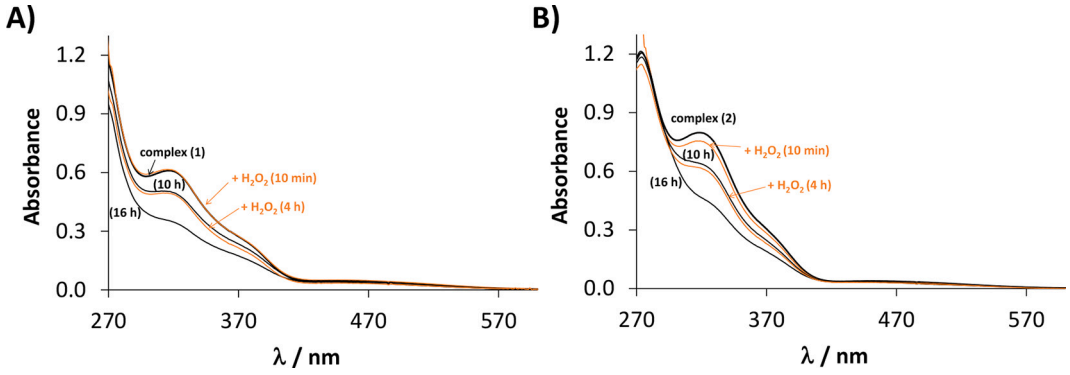

Fig. 7. Time-dependent UV–visible spectra of complex **1** (33 μM) (**A**) and complex **2** (41 μM) (**B**) at pH 7.4 (in 30% (*v*/v) DMSO/H_2O, 20 mM HEPES) after 10 and 16 h, and upon addition of 30 μl cc. H_2O_2 (spectra were recorded after 10 min and 4 h waiting time). (ℓ = 1 cm; T = 25 °C; I = 0.10 M KCl).

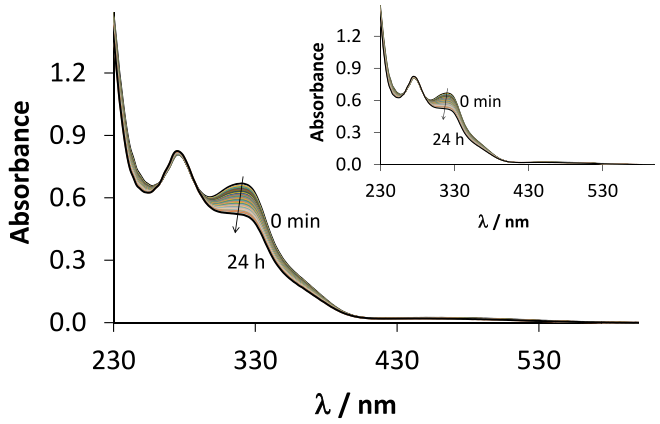

Fig. 8. Time-dependent changes of the UV–visible spectra of complex **1** and complex **2** (inserted figure) in ethanol. ($c_{complex}$ = 34 μM; ℓ = 1 cm; T = 25 °C; I = 0.10 M KCl).

lower IC_{50} and the higher TEAC values indicate stronger antioxidant effect. Based on the obtained data and the slow reaction, these complexes showed only a weak potential to act as antioxidant agents. It is noteworthy that the antioxidant property is considered as a chemoprotective feature; however numerous natural antioxidants and organometallic complexes were reported to display both antioxidant and anticancer activity [47–49].

4. Conclusion

All the studied compounds of formulation [Fe(η^5-C_5H_5)(k^2-dppe)(L)][CF_3SO_3] (**1–5**) (L = benzonitriles (**1–4**) or carbon monoxide (**5**)), [Fe(η^5-C_5H_5)(CO)(PPh_3)$_2$][CF_3SO_3] (**6**) and [Fe(η^5-C_5H_5)(CO)(PPh_3)(benzonitriles)][CF_3SO_3] (**7–9**) revealed high cytotoxicity against the human colon adenocarcinoma cell lines Colo205 and the refractile Colo320 with IC_{50} values in the micromolar range. Structure-activity studies indicate that, for the benzonitrile-based compounds, the dppe ligand in the coordination sphere led to more cytotoxic compounds showing, in most cases, selectivity against resistant cells and higher selectivity towards cancer cells (vs. embryonic fibroblasts). The rhodamine 123 accumulation assay revealed that the selectivity towards resistant cells is not related to ABCB1 inhibition. Complexes **1** and **2** presented the best redox behaviour on the cyclic voltammetry studies with a good stability on the pair Fe(III)/Fe(II) and were selected for monitoring their reactivity with endogenous reducing and oxidizing agents, namely with GSH and H_2O_2. The complexes exhibited no interaction with GSH, meanwhile their slow oxidation was observed in the presence of atmospheric O_2, a process that was further accelerated by the presence of H_2O_2. As the complexes acted as reducing agents, their antioxidant capacity was also assayed. They demonstrated the ability to quench the DPPH radical through a slow reaction with relatively high IC_{50} values indicating a weak antioxidant capacity.

Overall, compound **2**, bearing 4-aminobenzonitrile stands out as a lead for this family of compounds and further studies to try to unveil its mechanism of action will be performed.

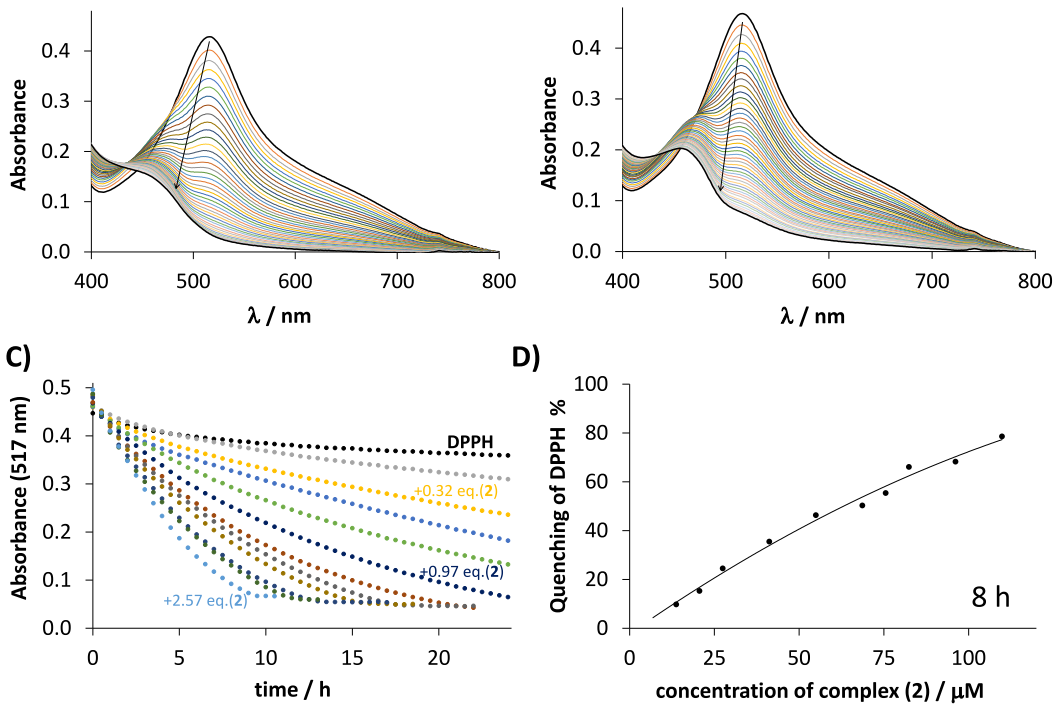

Fig. 9. Time-dependent changes of the UV–visible spectra of the DPPH radical in the presence of one equivalent of complex **1** (**A**) and complex **2** (**B**) in ethanol. Absorbance changes of DPPH at 517 nm upon reaction with complex **2** at different concentrations in ethanol plotted against time (**C**). Quenching of the DPPH radical at different concentrations of complex **2** at 8 h waiting time (**D**). (c_{DPPH} = 41.8 µM; $c_{complex}$ = 0–107.5 µM; ℓ = 1 cm; T = 25 °C; I = 0.10 M KCl).

Authors statement

All the authors have seen and approved the final version of the manuscript being submitted to Journal of Inorganic Biochemistry. The article is the authors' original work, hasn't received prior publication and isn't under consideration for publication elsewhere.

Declaration of Competing Interest

The authors declare that they have no known competing financial interests or personal relationships that could have appeared to influence the work reported in this paper.

Data availability

Data will be made available on request.

Acknowledgments

This work was funded by *Fundação para a Ciência e a Tecnologia* (FCT), I.P./MCTES through national funds (PIDDAC) - UIDB/00100/2020, UIDP/00100/2020 and LA/P/0056/2020. Andreia Valente acknowledges CEECIND 2017 (CEECIND/01974/2017; acknowledging FCT, as well as POPH and FSE—European Social Fund). A. P. thank FCT for his Ph.D. Grant (SFRH/BD/139412/2018 and COVID/BD/153267/2023). B.R. was supported by the Szeged Foundation for Cancer Research (Szegedi Rákkutatásért Alapítvány). G.S. was supported by the János Bolyai Research Scholarship (BO/00158/22/5) of the Hungarian Academy of Sciences and by the ÚNKP-22-5-SZTE-588 New National Excellence Program of the Ministry for Culture and Innovation from the source of the National Research, Development and Innovation Fund.

Appendix A. Supplementary data

Supplementary data to this article can be found online at https://doi.org/10.1016/j.jinorgbio.2023.112386.

References

[1] M. Bouché, C. Hognon, S. Grandemange, A. Monari, P.C. Gros, Dalton Trans. 49 (2020) 11451–11466.
[2] E.J. Anthony, E.M. Bolitho, H.E. Bridgewater, O.W.L. Carter, J.M. Donnelly, C. Imberti, E.C. Lant, F. Lermyte, R.J. Needham, M. Palau, P.J. Sadler, H. Shi, F.-X. Wang, W.-Y. Zhang, Z. Zhang, Chem. Sci. 11 (2020) 12888–12917.
[3] E.J. Anthony, E.M. Bolitho, H.E. Bridgewater, O.W.L. Carter, J.M. Donnelly, C. Imberti, E.C. Lant, F. Lermyte, R.J. Needham, M. Palau, P.J. Sadler, H. Shi, F. X. Wang, W.Y. Zhang, Z. Zhang, Chem. Sci. 11 (2020) 12888–12917.
[4] M.M. González-Ballesteros, C. Mejía, L. Ruiz-Azuara, FEBS Open Bio 12 (2022) 880–899.
[5] D. Baecker, B.N. Ma, J. Sagasser, L. Schultz, C. Hörschläger, M. Weinreich, L. Steiner, B. Kircher, R. Gust, Dalton Trans. 49 (2020) 6842–6853.
[6] G. Jaouen, A. Vessières, S. Top, Chem. Soc. Rev. 44 (2015) 8802–8817.
[7] I.A. Jaiyesimi, A.U. Buzdar, D.A. Decker, G.N. Hortobagyi, J. Clin. Oncol. 13 (1995) 513–529.
[8] P. Resnier, N. Galopin, Y. Sibiril, A. Clavreul, J. Cayon, A. Briganti, P. Legras, A. Vessières, T. Montier, G. Jaouen, J.P. Benoit, C. Passirani, Pharmacol. Res. 126 (2017) 54–65.
[9] E. Allard, N.T. Huynh, A. Vessières, P. Pigeon, G. Jaouen, J.P. Benoit, C. Passirani, Int. J. Pharm. 379 (2009) 317–323.
[10] A. Valente, S. Royer, M. Narendra, T.J.L. Silva, P.J.G. Mendes, M.P. Robalo, M. Abreu, J. Heck, M.H. Garcia, J. Organomet. Chem. 736 (2013) 42–49.
[11] R.D. Theys, M.E. Dudley, M.M. Hossain, Coord. Chem. Rev. 253 (2009) 180–234.
[12] M. Natarajan, X. Li, W. Zhong, W. Wang, Z. Xiao, X. Jiang, C. Lu, X. Liu, Electrochim. Acta 433 (2022) 141207.
[13] T.F. Wang, J.P. Juang, Y.S. Wen, J. Organomet. Chem. 503 (1995) 117–128.
[14] M.H. Garcia, P. Florindo, M.F.M. Piedade, M.T. Duarte, M.P. Robalo, J. Heck, C. Wittenburg, J. Holtmann, E. Licandro, J. Organomet. Chem. 693 (2008) 2987–2999.
[15] A. Valente, S. Royer, M. Narendra, T.J.L. Silva, P.J.G. Mendes, M.P. Robalo, M. Abreu, J. Heck, M.H. Garcia, J. Organomet. Chem. 736 (2013) 42–49.
[16] D. Astruc, E. Boisselier, C. Ornelas, Chem. Rev. 110 (2010) 1857–1959.
[17] A. Pilon, F. Avecilla, M. Mohai, É.A. Enyedy, B. Rácz, G. Spengler, M.H. Garcia, A. Valente, Eur. J. Med. Chem. 256 (2023), 115466.
[18] A.C. Gonçalves, T.S. Morais, M.P. Robalo, F. Marques, F. Avecilla, C.P. Matos, I. Santos, A.I. Tomaz, M.H. Garcia, J. Inorg. Biochem. 129 (2013) 1–8.
[19] H.T. Poh, P.C. Ho, W.Y. Fan, RSC Adv. 6 (2016) 18814–18823.
[20] S. Braccini, G. Provinciali, L. Biancalana, G. Pampaloni, F. Chiellini, F. Marchetti, Appl. Sci. 11 (2021) 4351 (10 pages).
[21] P.R. Florindo, D.M. Pereira, P.M. Borralho, C.M.P. Rodrigues, M.F.M. Piedade, A. C. Fernandes, J. Med. Chem. 58 (2015) 4339–4347.
[22] A. Benamrane, B. Herry, V. Vieru, S. Chakraborty, S. Biswas, S. Prince, C. Marschner, B. Blom, J. Organomet. Chem. 934 (2021) 121659.

[23] A. Pilon, A.R. Brás, L. Côrte-Real, F. Avecilla, P.J. Costa, A. Preto, M. Helena Garcia, A. Valente, Molecules 25 (2020) 1592 (22 pages).
[24] A. Valente, A.M. Santos, L. Côrte-Real, M.P. Robalo, V. Moreno, M. Font-Bardia, T. Calvet, J. Lorenzo, M.H. Garcia, J. Organomet. Chem. 756 (2014) 52–60.
[25] A. Pilon, P. Gírio, G. Nogueira, F. Avecilla, H. Adams, J. Lorenzo, M.H. Garcia, A. Valente, J. Organomet. Chem. 852 (2017) 34–42.
[26] D. Rocco, N. Busto, C. Pérez-Arnaiz, L. Biancalana, S. Zacchini, G. Pampaloni, B. Garcia, F. Marchetti, Appl. Organomet. Chem. 34 (2020) 1–18.
[27] G. Agonigi, L. Biancalana, M.G. Lupo, M. Montopoli, N. Ferri, S. Zacchini, F. Binacchi, T. Biver, B. Campanella, G. Pampaloni, V. Zanotti, F. Marchetti, Organometallics 39 (2020) 645–657.
[28] O.A. Lenis-Rojas, S. Cordeiro, M. Horta-Meireles, J.A.A. Fernández, S.F. Vila, J. A. Rubiolo, P. Cabezas-Sainz, L. Sanchez, A.R. Fernandes, B. Royo, Molecules 26 (2021) 1–14.
[29] S. Schoch, S. Braccini, L. Biancalana, A. Pratesi, T. Funaioli, S. Zacchini, G. Pampaloni, F. Chiellini, F. Marchetti, Inorg. Chem. Front. 9 (2022) 5118–5139.
[30] A. Valente, T.S. Morais, R.G. Teixeira, C.P. Matos, A.I. Tomaz, M. Helena Garcia, Synthetic Inorganic Chemistry: New Perspectives, 2021, pp. 223–276.
[31] M.H. Garcia, M.P. Robalo, A.R. Dias, M.F.M. Piedade, A. Galvão, W. Wenseleers, E. Goovaerts, J. Organomet. Chem. 619 (2001) 252–264.
[32] R.B. King, F.G.A. Stone, W.L. Jolly, G. Austin, W. Covey, D. Rabinovich, H. Steinberg, R. Tsugawa, Inorganic Syntheses Volume 7, 1963.
[33] T.S. Piper, G. Wilkinson, J. Inorg. Nucl. Chem. 2 (1956) 38–45.
[34] G.M. Sheldrick, SADABS, version 2.10, University of Göttingen, Germany, 2004.
[35] L.J. Bourhis, O.V. Dolomanov, R.J. Gildea, J.A.K. Howard, H. Puschmann, Acta Crystallogr, Sect. A Found. Crystallogr. 71 (2015) 59–75.
[36] O.V. Dolomanov, L.J. Bourhis, R.J. Gildea, J.A.K. Howard, H. Puschmann, J. Appl. Crystallogr. 42 (2009) 339–341.
[37] G.M. Sheldrick, Acta Crystallogr, Sect. C Struct. Chem. 71 (2015) 3–8.
[38] F. Xiao, T. Xu, B. Lu, R. Liu, Food Front. 1 (2020) 60–69.
[39] H. Adams, S.C.M. Agustinho, B.E. Mann, S. Smith, J. Organomet. Chem. 607 (2000) 175–181.
[40] A.R. Dias, M.H. Garcia, J.C. Rodrigues, M.L.H. Green, S.M. Kuebler, J. Organomet. Chem. 475 (1994) 241–245.
[41] R.G. Strickley, Pharm. Res. 21 (2004) 201–230.
[42] Y. Xi, P. Xu, Transl. Oncol. 14 (2021) 101174.
[43] S.A.R. Sancha, N. Szemerédi, G. Spengler, M.J.U. Ferreira, Int. J. Mol. Sci. 24 (2023) 2061.
[44] P. Kannan, S. Telu, S. Shukla, S.V. Ambudkar, V.W. Pike, C. Halldin, M. M. Gottesman, R.B. Innis, M.D. Hall, ACS Chem. Neurosci. 2 (2011) 82–89.
[45] A.L. Ortega, S. Mena, J.M. Estrela, Cancers (Basel). 3 (2011) 1285–1310.
[46] W. Brand-Williams, M.E. Cuvelier, C. Berset, LWT - food Sci, Technol. 28 (1995) 25–30.
[47] I. Grigalius, V. Petrikaite, Molecules 22 (2017) 2169 (12 pages).
[48] J. Ceramella, R. Troiano, D. Iacopetta, A. Mariconda, M. Pellegrino, A. Catalano, C. Saturnino, S. Aquaro, M.S. Sinicropi, P. Longo, Antibiotics 12 (2023) 693 (20 pages).
[49] M. Małecka, A. Skoczyńska, D.M. Goodman, C.G. Hartinger, E. Budzisz, Coord. Chem. Rev. 436 (2021) 213849 (20 pages).